Drag reduction by polymer additives in a turbulent channel flow

By TAEGEE MIN[1], JUNG YUL YOO[2], HAECHEON CHOI[1,2], AND DANIEL D. JOSEPH[3]

[1]Center for Turbulence and Flow Control Research, Institute of Advanced Machinery and Design, Seoul National University, Seoul 151-742, Korea

[2]School of Mechanical and Aerospace Engineering, Seoul National University, Seoul 151-742, Korea

[3]Department of Aerospace Engineering and Mechanics, University of Minnesota, 107 Akerman Hall, 110 Union Street SE, Minneapolis, MN 55455, USA

(Received ?? and in revised form ??)

Turbulent drag reduction by polymer additives in a channel is investigated using direct numerical simulation. The dilute polymer solution is expressed with an Oldroyd-B model that shows a linear elastic behavior. Simulations are carried out by changing the Weissenberg number at the Reynolds numbers of 4000 and 20000 based on the bulk velocity and channel height. The onset criterion for drag reduction predicted in the present study shows a good agreement with previous theoretical and experimental studies. In addition, the flow statistics such as the rms velocity fluctuations are also in good agreements with previous experimental observations. The onset mechanism of drag reduction is interpreted based on the elastic theory that is one of the most plausible hypotheses suggested in the past. Therefore, the transport equations for the kinetic and elastic energy are derived for the first time. It is observed that the polymer stores the elastic energy from the flow very near the wall and then releases it there when the relaxation time is short, showing

no drag reduction. However, when the relaxation time is long enough, the elastic energy stored in the very near-wall region is transported to and released in the buffer and log layers, showing a significant amount of drag reduction.

---

1. Introduction

Since Toms (1949) reported turbulent drag reduction by polymer additives, there have been many studies on this phenomenon including theoretical, experimental and numerical approaches. The two important findings from experimental studies by Virk *et al.* (1967) and Virk (1971) are the onset of drag reduction and the existence of maximum drag reduction (MDR), suggesting that drag reduction does not come from a purely viscous effect of the dilute polymer solution (De Gennes 1990). That is, if the viscosity were a dominant parameter for drag reduction, the drag would decrease regardless of the amount of polymer concentration. However, experimental studies have shown the existence of a threshold concentration for drag reduction.

The first theoretical hypothesis about the onset of drag reduction is the 'time criterion' (Tulin 1966; Hershey & Zakin 1967; Lumley 1969). The time criterion indicates that drag reduction occurs when the relaxation time is longer than the time scale of the near-wall turbulence: i.e.,

$$\lambda > \frac{\nu}{u_\tau^2}, \tag{1.1}$$

where λ is the relaxation time, ν the kinematic viscosity of solution, $u_\tau = \sqrt{\tau_w/\rho}$ the wall shear velocity, τ_w the wall shear stress, and ρ the density of solution. The time criterion (1.1) was verified in the experiment of Berman (1977). Lumley (1973) explained that drag reduction comes from the elongational viscosity which is increased greatly by

'coil-stretch' transition under the condition of (1.1). Hinch (1977) showed theoretically that the 'coil-stretch' transition results in a great increase in the elongational viscosity. However, the scenario of the elongational viscosity was criticized in that the 'coil-stretch' does not occur in turbulent flow with randomly fluctuating strain rates (De Gennes 1990; Smith & Chu 1998; Sreenivasan & White 2000).

On the other hand, Goldshtik *et al.* (1982) applied a perturbation method to viscoelastic models (Maxwell and Oldroyd-B models) and showed that drag reduction occurs when

$$We_\tau = \frac{\lambda u_\tau^2}{\nu} > \alpha. \tag{1.2}$$

where We_τ is the Weissenberg number normalized by u_τ and ν, and α depends on the viscoelastic model. Here, (1.2) is a similar expression to (1.1). However, it should be noted that (1.2) does not come from the concept of the elongational viscosity but from the concept of the elasticity. They suggested that the time criterion may come from the elastic effect of dilute polymer solution.

Some experimental studies (for example, Gyr & Tsinober 1997; Den Toonder *et al.* 1997; Warholic *et al.* 1999) reported the existence of 'stress deficit' in drag reducing flow: i.e.

$$T_{12} > \mu \frac{d\overline{u}}{dy} - \rho\overline{u'v'}, \tag{1.3}$$

where T_{12} is the total shear stress ($= \mu d\overline{u}/dy - \rho\overline{u'v'} + \tau_p$), μ the viscosity of solution, $\overline{u}$ the mean streamwise velocity, $-\rho\overline{u'v'}$ the Reynolds shear stress, and τ_p the time-averaged stress deficit. This suggests that the viscoelasticity should be the most important property of dilute polymer solution for drag reduction because the elongational-viscosity hypothesis cannot show the existence of the stress deficit (Den Toonder *et al.* 1997).

In the mean time, de Gennes (1990) suggested an elastic theory for drag reduction that

was more elaborated by Sreenivasan & White (2000), in which the polymer molecules absorb the small-scale turbulence energy into the elastic energy and prohibit the turbulence cascade, resulting in drag reduction. Because the elastic theory did not concern itself with the wall region, de Gennes (1990) suggested that drag reduction might occur before polymer molecules, injected into the core of the pipe or channel flow, reached the wall. However, a recent experiment by Cadot *et al.* (1998) has shown that the wall effect is important for the polymer drag reduction.

Joseph (1990) also noted that the elasticity plays a predominant role in drag reduction. He thought that polymers always attenuate turbulence at small scales, and thus there should exist a natural cut-off scale provided by the shear wave speed u_c. Therefore, he suggested a criterion for drag reduction such as (see Joseph & Christodoulou 1993)

$$u_\tau > u_c = \sqrt{\frac{\nu}{\lambda}}. \tag{1.4}$$

Note that (1.4) is also the same as (1.1) and (1.2). Because the shear velocity u_τ is associated with the near-wall turbulence, the Joseph's hypothesis on the elasticity can be linked with the wall turbulence.

Recently, researches conducted using direct numerical simulation (DNS) (Orlandi 1995; Den Toonder *et al.* 1997; Sureshkumar *et al.* 1997; Dimitropoulos *et al.* 1998) provided more information about the polymer drag reduction. Orlandi (1995) and den Toonder *et al.* (1997) adopted elongational viscosity models and obtained drag reduction. However, such models are based on inelastic constitutive equations, and thus cannot predict the onset of drag reduction and the 'stress deficit'. More recently, Sureshkumar *et al.* (1997) and Dimitropoulos *et al.* (1998) adopted viscoelastic models (FENE-P† and Giesekus models) and used an artificial diffusion scheme (AD) for the spatial discretization of the

† FENE stands for "finitely extensible, non-linear elastic".

convection term in their constitutive equations. However, this scheme smears out the steep gradients of polymer stresses, resulting in less drag reduction. Therefore they had to introduce a larger elasticity to obtain an appropriate amount of drag reduction (see Min *et al.* 2001). In addition, none of those studies did not explain how the elasticity causes drag reduction.

The objective of the present study is to propose a mechanism responsible for drag reduction by polymer additives using DNS of turbulent flow in a channel. An Oldroyd-B model (linear Hookean dumbbells) is used to represent the behaviour of polymer. The Reynolds numbers used in the previous studies using DNS were regarded too small as compared with those used in the experimental studies (Gyr & Tsinober 1997; Sreenivasan & White 2000). Therefore, in the present study, simulations are conducted for $Re_b = U_b h/\nu = 4000$ (same order of magnitude as previous DNS studies) and $Re_b = 20000$ (same order of magnitude as previous experimental studies) based on the bulk velocity U_b and channel height h. The results are compared with the previous experimental studies. Moreover, the transport equations for the kinetic and elastic energy are derived for the first time by using the 'elastic theory' of Tabor & de Gennes (1986). Energy transfer between the flow and the polymer is examined through the kinetic and elastic energy transport equations, from which the mechanism for drag reduction is elucidated.

2. Governing equations and numerical method

The non-dimensional governing equations of unsteady incompressible viscoelastic flow with an Oldroyd-B model are as follows:

$$\frac{\partial u_i}{\partial t} + \frac{\partial}{\partial x_j}(u_i u_j) = -\frac{\partial p}{\partial x_i} + \frac{\beta}{Re}\frac{\partial^2 u_i}{\partial x_j \partial x_j} + \frac{1-\beta}{Re}\frac{\partial \tau_{ij}}{\partial x_j}, \tag{2.1}$$

$$\frac{\partial u_i}{\partial x_i} = 0, \tag{2.2}$$

$$\tau_{ij} + We(\frac{\partial \tau_{ij}}{\partial t} + u_m \frac{\partial \tau_{ij}}{\partial x_m} - \frac{\partial u_i}{\partial x_m}\tau_{mj} - \frac{\partial u_j}{\partial x_m}\tau_{mi}) = \frac{\partial u_i}{\partial x_j} + \frac{\partial u_j}{\partial x_i}, \tag{2.3}$$

where u_i is the velocity, p the pressure, τ_{ij} the polymer stress, Re $(= U\delta/\nu)$ the Reynolds number, We $(= \lambda U/\delta)$ the Weissenberg number, U the centerline velocity of the fully developed laminar flow $(U = \frac{3}{2}U_b)$, δ the channel half height $(\delta = \frac{1}{2}h)$, and β is the ratio of solvent viscosity contribution to total viscosity of solution. In the present study, β is fixed to be 0.9 for the case of a viscoelastic fluid, because the dilute solutions that give rise to drag reduction are nearly Newtonian in a sense that they have essentially the same viscosity as the solvent. For $Re = 3000$ $(Re_b = U_b h/\nu = 4000; Re_\tau = u_{\tau_0}\delta/\nu \simeq 135)$, a calculation domain of $7\delta \times 2\delta \times 3.5\delta$ is chosen in the streamwise (x), wall-normal (y) and spanwise (z) directions, respectively, with $64 \times 97 \times 96$ grids $(\Delta x^+ \simeq 15,\ \Delta y^+_{min} \simeq 0.3,$ $\Delta z^+ \simeq 5)$. Here u_{τ_0} is the wall shear velocity for Newtonian fluid flow $(\beta = 1)$. For $Re =$ 15000 $(Re_b = 20000; Re_\tau \simeq 530)$, the minimal channel concept by Jiménez and Moin (1991) is adopted† and a calculation domain of $2.4\delta \times 2\delta \times 0.9\delta$ is chosen with $128 \times 257 \times 96$ grids $(\Delta x^+ \simeq 10,\ \Delta y^+_{min} \simeq 0.4,\ \Delta z^+ \simeq 5)$. The grid resolution used is almost the same as that of Moser *et al.* (1999). We impose the periodic boundary condition in the streamwise and spanwise directions, and the no-slip boundary condition in the wall-

† For larger Weissenberg numbers leading to near maximum drag reduction (MDR), this minimal channel concept is no more valid because the turbulence structures become very large at the MDR state (Min *et al.* 2002).

normal direction. A fully developed turbulent flow field of a Newtonian fluid ($\beta = 1$) is used as an initial condition for the simulation of viscoelastic fluid flow. A constant mass flow rate is maintained in a channel during simulation by adjusting the mean pressure gradient at each computational time step. In other words, the bulk Reynolds number (Re_b) is constant during simulation.

The numerical algorithm is based on a semi-implicit, fractional step method: the velocity diffusion and polymer stress derivative terms in (2.1) are advanced with the Crank-Nicolson method, and the velocity convection term in (2.1) and all the terms in (2.3) are advanced with a third-order Runge-Kutta method. A fourth-order compact difference scheme (COM4; Lele 1992) is used for the polymer stress derivative $\partial\tau_{ij}/\partial x_j$ in (2.1), and a modified compact upwind difference scheme (MCUD3; Min *et al.* 2001) is used for the polymer-stress convection term $u_m\partial\tau_{ij}/\partial x_m$ in (2.3). All other terms are discretized using the second-order central difference (CD) scheme. Here, we briefly introduce COM4 and MCUD3 in this paper (For the detailed feature of the present numerical method, see Min *et al.* 2001).

The spatial derivative of τ_{ij} in (2.1) is obtained using COM4: e.g.

$$\left.\frac{\partial\tau_{ij}}{\partial x}\right|^{q+1} + 4\left.\frac{\partial\tau_{ij}}{\partial x}\right|^{q} + \left.\frac{\partial\tau_{ij}}{\partial x}\right|^{q-1} = \frac{3}{\Delta}\left(\tau_{ij}^{q+1} - \tau_{ij}^{q-1}\right) + O\left(\Delta^4\right), \tag{2.4}$$

where q is the index of a grid cell and Δ is the grid spacing. (2.4) results in a tridiagonal matrix system, so one can easily obtain a fourth-order accuracy for $\partial\tau_{ij}/\partial x$. The spatial derivative of τ_{ij} in (2.3) is obtained using a third-order compact upwind difference scheme (CUD3, Tolstykh & Lipavskii 1998): e.g.

$$\left(2 - 3s^{q+\frac{1}{2}}\right)\left.\frac{\partial\tau_{ij}}{\partial x}\right|^{q+1} + \left(8 - 3s^{q+\frac{1}{2}} + 3s^{q-\frac{1}{2}}\right)\left.\frac{\partial\tau_{ij}}{\partial x}\right|^{q} + \left(2 + 3s^{q-\frac{1}{2}}\right)\left.\frac{\partial\tau_{ij}}{\partial x}\right|^{q-1} \tag{2.5}$$

$$= \frac{6}{\Delta}\left[\left(1 - s^{q+\frac{1}{2}}\right)\tau_{ij}^{q+1} + \left(s^{q+\frac{1}{2}} + s^{q-\frac{1}{2}}\right)\tau_{ij}^{q} - \left(1 + s^{q-\frac{1}{2}}\right)\tau_{ij}^{q-1}\right] + O\left(\Delta^3\right),$$

where $s^{q+\frac{1}{2}}$ is the sign of the x-component velocity (u) between the q-th and $(q+1)$-th cells, that is, $s^{q+\frac{1}{2}} = 1$ when $u^{q+\frac{1}{2}} \geqslant 0$, and $s^{q+\frac{1}{2}} = -1$ when $u^{q+\frac{1}{2}} < 0$. Here in CUD3, an upwinding is introduced to COM4 in order to have a dissipative error. When $s = 0$, CUD3 is equal to COM4.

It is known that the configuration tensor c_{ij} $(= We \cdot \tau_{ij} + \delta_{ij})$ loses its positive definiteness due to the accumulation of numerical errors, which results in the numerical breakdown (Joseph 1990; Min *et al.* 2001). Thus, in MCUD3, we add a second-order artificial diffusion scheme (AD) to CUD3 at each time step at the locations where the determinant of the configuration tensor becomes negative, in order to prevent the numerical instability at an initial stage. The effect of the dissipative error caused by this AD on the flow field is negligible because the grid locations where AD is added change in time and the number of the corresponding grid points is very small (at most less than 0.5%) for the present flow. Recently, MCUD3 was successfully utilized in the study of Dubief & Lele (2001).

One might wonder if the resolution required for the simulation of viscoelastic fluid flow should be higher than that for the simulation of Newtonian fluid flow. In our study, we confirmed from simulation that for the present flow the polymeric stress derivatives in (2.1), $\frac{1-\beta}{Re}\frac{\partial \tau_{ij}}{\partial x_j}$, are the same order of magnitude as the Newtonian stress derivatives, $\frac{\beta}{Re}\frac{\partial^2 u_i}{\partial x_j \partial x_j}$. Thus, with the same resolution used for the Newtonian fluid flow, the use of COM4 for the polymeric stress derivatives in (2.1) and that of MCUD3 for the polymer-stress convection term in (2.3) should be enough to resolve the spatial distribution of the polymeric stresses. Furthermore, as we will show in the next section, our simulation results agree very well with the previous experimental results for the present flow, and

the power spectra of the polymeric stresses do not show any power pile-up at high wavenumbers. Nevertheless, it should be noted that the present low-order schemes used for the spatial derivatives may require higher resolution to obtain high-order turbulence statistics (Choi *et al.* 1992).

We have also separately simulated the same flow with a different viscoelastic model, FENE-P model, to see how the unboundedness of the polymer stretch in the Oldroyd-B model affects the drag and velocity field. In appendix, we clearly show that the Oldroyd-B model does not produce any unbounded polymer stretch at least for the present flow, and the drag and rms velocity fluctuations are nearly the same as those obtained from the FENE-P model (see appendix for the detail).

Re†	We‡	We_τ	DR (%)
3000	0.1	0.60	0
	0.5	3.0	0
	1	6.0	0
	2	12	12
	3	18	20
	4	24	27
15000	0.2	3.7	0
	0.3	5.6	0
	0.5	9.3	8
	1	19	21
	2	37	28

† $Re_b = U_b h/\nu = \frac{4}{3}Re$
‡ $We_b = \lambda U_b/h = \frac{1}{3}We$

TABLE 1. Variation of the drag with respect to the Weissenberg number at $Re = 3000$ and 15000

3. Changes in the quantities of flow variables

3.1. *Drag variation and onset criterion of drag reduction*

Figure 1 shows the time histories of the mean pressure gradient to drive a constant mass flow rate in a channel at $Re = 3000$ and 15000, normalized by that of Newtonian fluid flow ($-d\overline{p}/dx|_0$). The percentage of drag reduction (DR) is defined as

$$DR = \frac{\left(-\frac{d\overline{p}}{dx}\Big|_0\right) - \left(-\frac{d\overline{p}}{dx}\right)}{-\frac{d\overline{p}}{dx}\Big|_0} \times 100. \tag{3.1}$$

Table 1 shows the variation of the drag with respect to the Weissenberg number. It is seen that drag reduction occurs at $We > 1$ and $We > 0.3$, respectively, for $Re = 3000$ and 15000, and the drag decreases more with larger Weissenberg number. The drag does neither decrease nor increase at $We = 0.1$, 0.5 and 1 for $Re = 3000$ and at $We = 0.2$ and 0.3 for $Re = 15000$, respectively. This indicates that there exists a threshold for

the Weissenberg number to achieve drag reduction. The onset Weissenberg number We_τ normalized by u_{τ_0} and ν for drag reduction is about 6 for both Reynolds numbers.

The 'time criterion' suggested by Lumley (1969) indicated that the onset We_τ for drag reduction is 1. Berman (1977) showed that the onset We_τ ranges from 1 to 8 depending on the properties of polymers and solvents. Goldshtik *et al.* (1982) studied the polymer drag reduction theoretically and suggested that the onset We_τ is 1 for the Maxwell model and $5 \sim 6$ for the Oldroyd-B model with $\beta = 0.9$.

Orlandi (1995) and den Toonder *et al.* (1997) could not predict the onset We_τ from their direct numerical simulations because they used inelastic constitutive models. Sureshkumar *et al.* (1997) and Dimitropoulos *et al.* (1998) showed that drag reduction occurred at $We_\tau = 25$ but did not at $We_\tau = 12.5$. This Weissenberg number is much larger than the onset Weissenberg number obtained from experimental and theoretical studies. As mentioned previously, the numerical schemes used in Sureshkumar *et al.* (1997) and Dimitropoulos *et al.* (1998) smear out the steep gradient of polymer stresses, which may result in less or no drag reduction at a Weissenberg number larger than the threshold Weissenberg number (see also Min *et al.* 2001). On the other hand, the onset Weissenberg number obtained from the present study shows an excellent agreement with previous theoretical and experimental results.

3.2. *Mean velocity and turbulence intensities*

The mean velocity profiles normalized by the actual wall-shear velocity u_τ are shown in figure 2, together with the experimental results by Luchik & Tiederman (1988) and Wei & Willmarth (1992). Here, $u^+ = \overline{u}/u_\tau$, $y^+ = yu_\tau/\nu$, and $\overline{u}$ is the mean streamwise velocity. It is hard to compare numerical results with experimental ones, because the parameters in the constitutive equations are not easy to obtain from the polymer used in the experiments (Joseph 1990). However, the experimental studies in Luchik & Tie-

derman (1988) and Wei & Willmarth (1992) were conducted at the Reynolds numbers of $Re_\tau \simeq 520$ and 570, respectively, which are very similar to that of the present study ($Re_\tau \simeq 530$). Furthermore, the amounts of drag reduction reported in Luchik & Tiederman (1988) and Wei & Willmarth (1992) are, respectively, 20% and 30%, which are also nearly identical to those obtained in the present study (21% and 28% for $We = 1$ and 2, respectively). Therefore, the results from two experimental studies are compared with the present ones in figure 2.

It is evident from figure 2 that the mean velocity profiles agree very well with the experimental results. Also, upward shifts in the log-law are clearly observed for the drag-reducing flows, which has been observed in other types of drag-reducing flows such as a flow over riblets (Choi *et al.* 1993) and a flow with active blowing and suction (Choi *et al.* 1994). It is also noticeable from figure 2 that the viscous sublayer thickness (VST) increases for the drag-reducing flows (we also confirmed this finding from the plot of u^+/y^+ vs. y^+), which has been previously observed in the experimental studies (Luchik & Tiederman 1988; Wei & Willmarth 1992). Goldshtik *et al.* (1982) reported that the VST does not change for the Maxwell model ($\beta = 0$) and the Oldroyd-B model with a short retardation time such as $\beta = 0.2$, but it increases for the Oldroyd-B model with a long retardation time such as $\beta = 0.9$ and 0.95. Therefore, the increase in the VST from the present study also shows a good agreement with the theory of Goldshtik *et al.* (1982) because $\beta = 0.9$ for the present study.

Variation of the root-mean-square (rms) velocity fluctuations with the Weissenberg number is shown in figure 3, together with the experimental results by Luchik & Tiederman (1988) and Wei & Willmarth (1992). As the Weissenberg number increases, the rms streamwise velocity fluctuations decrease very near the wall but increase away from the wall, whereas the rms wall-normal and spanwise velocity fluctuations decrease in the

whole channel. It is seen that the present results are also in good agreements with the experimental results of Luchik & Tiederman (1988) and Wei & Willmarth (1992). The increase in u_{rms} in a drag-reducing flow was also observed in a turbulent channel flow with a streamwise magnetic field (Lee & Choi 2001), whereas the decrease in u_{rms} was observed in a flow above riblets (Choi *et al.* 1993) and a flow with active blowing and suction (Choi *et al.* 1994), indicating that the variation of u_{rms} is not a direct indication of drag reduction. Warholic *et al.* (1999) also reported the decrease in u_{rms} in the case of large drag reduction for polymer turbulent flow, while u_{rms} increases in the case of small drag reduction. On the other hand, the rms cross-velocity fluctuations decreased for all the drag-reducing flows. The turbulent kinetic energy showed the same trend as the rms streamwise velocity fluctuations (not shown here), because u_{rms} is much larger than v_{rms} and w_{rms}.

Variation of the rms vorticity fluctuations with the Weissenberg number is shown in figure 4. All three components of the vorticity fluctuations substantially decrease with increasing Weissenberg number. It is also noticeable that the y-location of the local maximum of the streamwise vorticity fluctuations moves further away from the wall with increasing Weissenberg number, which indicates that the streamwise-vortex center moves away from the wall in the turbulent flow of polymeric liquids and the sweep motion induced by those streamwise vortices is less effective in producing a high skin friction.

3.3. *Reynolds shear stress and stress deficit*

The Reynolds shear stress, $-\rho\overline{u'v'}$, and total shear stress, $T_{12} = \mu d\overline{u}/dy - \rho\overline{u'v'} + \tau_p$, normalized by u_{τ_0} are shown in figure 5, together with the Reynolds shear stress from the experimental studies by Luchik & Tiederman (1988) and Wei & Willmarth (1992). The total shear stress should be a straight line when the flow reaches a fully developed state, and the present result shows that this is indeed the case. The slope of the total

shear stress decreases with increasing Weissenberg number, because the mean pressure gradient required to drive a constant mass flux in a channel decreases (see figure 1). A significant reduction in the Reynolds shear stress is also observed throughout the channel with the polymer additives. It is seen that the present results of $-\overline{u'v'}$ are in good agreements with the experimental results of Luchik & Tiederman (1988). Note that the disagreement with the polymer case of Wei & Willmarth (1992) might come from their mistake in data implementation since the slope of their Reynolds shear stress in the channel center suggests much larger drag reduction (about 50%) than what they really obtained (30%).

One of the most interesting features in turbulent drag reduction of a dilute polymer solution is the 'stress deficit', which was already described as (1.3). For an Oldroyd-B model, (1.3) can be derived as

$$\begin{aligned} T_{12} &= \mu_N \frac{d\overline{u}}{dy} - \rho\overline{u'v'} + \overline{\tau}_{12} \\ &= \mu_N \frac{d\overline{u}}{dy} - \rho\overline{u'v'} + \mu_E \frac{d\overline{u}}{dy} + \tau_p \\ &= \mu \frac{d\overline{u}}{dy} - \rho\overline{u'v'} + \tau_p \end{aligned} \tag{3.2}$$

where μ_N is the Newtonian viscosity and μ_E the elastic viscosity. The Newtonian viscosity μ_N is not the solvent viscosity μ_s but is interpreted as an effective Newtonian contribution to the solution viscosity μ (see Joseph 1990, Chap. 18). It is not easy to measure the correct values of μ_N, whereas μ and μ_s can be easily measured by using a viscometer. Since we consider a dilute polymer solution where μ is almost the same as μ_s, (3.2) can be expressed as (see also Warholic *et al.* 1999),

$$T_{12} = \mu_s \frac{d\overline{u}}{dy} - \rho\overline{u'v'} + \tau_p. \tag{3.3}$$

The total shear stress normalized by the actual wall-shear velocity u_τ is

$$T_{12}^+ = \frac{du^+}{dy^+} - \overline{u'^+ v'^+} + \tau_p^+, \tag{3.4}$$

where τ_p^+ is the dimensionless stress deficit by polymer additives that cannot be predicted by an inelastic theory although it is observed experimentally (see den Toonder *et al.* 1997). Figure 6 shows the stress deficit obtained from the present study. The stress deficit increases with increasing Weissenberg number, and its maximum locates in the buffer layer, which was also reported in the experimental result by den Toonder *et al.* (1997). Note also that τ_p becomes large with increasing Reynolds number.

3.4. *Power spectra of the polymer stresses* τ_{11}, τ_{22} *and* τ_{33}

Figure 7 shows the power spectra of the polymer stresses, $(1-\beta)/Re \cdot \tau_{11}$, $(1-\beta)/Re \cdot \tau_{22}$ and $(1-\beta)/Re \cdot \tau_{33}$, at $Re = 3000$ for the cases of no drag reduction and 20% drag reduction. Here k_x and k_z are the streamwise and spanwise wavenumbers, respectively. The power spectra shown in this figure illustrate that the present grid resolution is adequate, because the power density at high wavenumbers is a few to several decades lower that the power density at low wavenumbers, and there is no evidence of power pile-up at high wavenumbers. At $y_0^+ \simeq 30$, all the polymer stresses increase with increasing Weissenberg number irrespective of drag reduction. However, at $y_0^+ \simeq 10$ (near the wall), τ_{11} and τ_{33} increase but τ_{22} decreases when drag reduction occurs. This phenomenon is in good agreement with the near-wall analysis of Goldshtik *et al.* (1982): the stretching stresses acting in the near-wall plane parallel to the wall (τ_{11} and τ_{33}) may damp out the near-wall wall-normal motion. These different behaviors of the polymer stretch at different wall-normal locations are closely associated with the present drag reduction mechanism which will be presented in the next section.

4. Drag reduction mechanism

The elastic theory is first suggested by Tabor & de Gennes (1986). They assumed that polymers in solvent behave like an elastic spring. When the spring is a linear one, the elastic energy per unit volume stored by polymers can be expressed as

$$k_p^* = \frac{1}{2} nG \left(\langle Q^2 \rangle - \langle Q^2 \rangle_{eq} \right), \tag{4.1}$$

where n is the number of polymer molecules per unit volume, G the elastic modulus, $\langle Q^2 \rangle$ the ensemble average of polymer length squared, and the subscript 'eq' denotes the equilibrium state. However, when the spring is not a linear one, the expression of (4.1) should be modified. For example, Pincus (1976) reported that the elastic energy is proportional to $\langle Q^{5/4} \rangle$ rather than $\langle Q^2 \rangle$ (see also de Gennes 1990 and Sreenivasan & White 2000). Since the polymer molecule in the Oldroyd-B model is regarded as a linear dumbbell, the non-linear elastic effect is neglected in the framework of the present approach.

From the kinetic theory (p. 72 in Bird *et al.* 1987), $\langle Q^2 \rangle$ and $\langle Q^2 \rangle_{eq}$ can be derived as follows:

$$\begin{aligned} \langle Q^2 \rangle &= \frac{3k_B T}{G} + \frac{\tau_{ii}^*}{nG}, \\ \langle Q^2 \rangle_{eq} &= \frac{3k_B T}{G}, \end{aligned} \tag{4.2}$$

where k_B is the Boltzmann constant, T is the absolute temperature, and τ_{ii}^* is the trace of the dimensional polymer stress. Then, k_p^* becomes

$$k_p^* = \frac{1}{2} \tau_{ii}^* \tag{4.3}$$

In a non-dimensional form, k_p^* becomes

$$k_p = \frac{1}{2}\frac{1-\beta}{Re}\tau_{ii}. \tag{4.4}$$

Using the definition of the elastic energy k_p in (4.4), one can obtain the transport equations for the kinetic and elastic energy from the momentum and constitutive equations as follows:

$$\left\langle \frac{Dk_m}{Dt} \right\rangle = -\langle P_k \rangle - \langle P_{e,m} \rangle + \langle P_w \rangle + \beta \left\langle \frac{1}{Re}\frac{d^2 k_m}{dy^2} \right\rangle - \beta \langle \epsilon_m \rangle, \tag{4.5}$$

$$\left\langle \frac{Dk_t}{Dt} \right\rangle = \langle P_k \rangle - \langle P_{e,t} \rangle + \beta \left\langle \frac{1}{Re}\frac{d^2 k_t}{dy^2} \right\rangle - \beta \langle \epsilon_k \rangle, \tag{4.6}$$

$$\left\langle \frac{Dk_e}{Dt} \right\rangle = \langle P_{e,m} \rangle + \langle P_{e,t} \rangle - \frac{1}{We} \langle k_e \rangle, \tag{4.7}$$

where

$$k_m = \frac{1}{2}\overline{u}^2,\ k_t = \frac{1}{2}\overline{u_i' u_i'},\ k_e = \overline{k}_p,$$

$$P_k = -\overline{u'v'}\frac{d\overline{u}}{dy},\ P_{e,m} = \frac{1-\beta}{Re}\overline{\tau}_{12}\frac{d\overline{u}}{dy},$$

$$P_w = -\overline{u}\frac{d\overline{p}}{dx},\ \epsilon_m = \frac{1}{Re}\frac{d\overline{u}}{dy}\frac{d\overline{u}}{dy},$$

$$P_{e,t} = \frac{1-\beta}{Re}\overline{\frac{\partial u_i'}{\partial x_j}\tau_{ij}'},\ \epsilon_k = \frac{1}{Re}\overline{\frac{\partial u_i'}{\partial x_j}\frac{\partial u_i'}{\partial x_j}}.$$

Here $\langle \cdot \rangle = (1/V)\int \cdot dV$ and V is the total volume of the computational domain. Equations (4.5)-(4.7) provide the information about the energy transfer between the polymer and the flow. The energy transfer between the mean kinetic energy k_m and the turbulent kinetic energy k_t is executed through P_k. The energy transfer between the mean kinetic energy k_m and the elastic energy k_e is done through $P_{e,m}$, and that between the turbulent kinetic energy k_t and the elastic energy k_e is done through $P_{e,t}$. The turbulent kinetic energy k_t is dissipated by ϵ_k and the elastic energy k_e is dissipated by itself.

Figure 8 shows the time histories of the volume-averaged production $\langle P_k \rangle$ and dissipation $\langle \epsilon_k \rangle$ of the turbulent kinetic energy. The mean values of $\langle P_k \rangle$ and $\langle \epsilon_k \rangle$ decrease with increasing We when drag reduction occurs, because turbulence inside the channel becomes weaker. However, it is interesting to note that the fluctuating amplitudes of $\langle P_k \rangle$ and $\langle \epsilon_k \rangle$ becomes larger as We increases. This phenomenon is associated with the temporal variation of the elastic energy which will be discussed later. The spatial distributions of P_k and ϵ_k are shown in figure 9. The production and dissipation of the turbulent kinetic energy decrease throughout the channel with the polymer additives.

Figure 10 shows the time histories of the volume-averaged productions, $\langle P_{e,m} \rangle$ and $\langle P_{e,t} \rangle$, and dissipation, $-\langle k_e \rangle / We$, of the elastic energy. In the case of no drag reduction ($We = 1$ and 0.3 for $Re = 3000$ and 15000, respectively), $\langle P_{e,m} \rangle$, $\langle P_{e,t} \rangle$ and $-\langle k_e \rangle / We$ are nearly constant in time, indicating that the energy transfer from the flow to the polymer is nearly steady and the amount of energy received from both the mean and turbulent kinetic energy is dissipated by the elastic energy itself (see (4.7)). Interestingly, as shown in figure 11, the values of $\langle P_{e,m} \rangle$, $\langle P_{e,t} \rangle$ and $-\langle k_e \rangle / We$ are nearly the same irrespective of We in the case of no drag reduction (i.e. in the case of $We \leqslant 1$ at $Re = 3000$). This means that the amount of energy transfer from the mean and turbulent kinetic energy to the elastic energy is the same irrespective of We in the case of no drag reduction, which again indicates that, with the polymer, $(1-\beta)$ times the dissipation and diffusion of the Newtonian fluid is replaced by $\langle P_{e,m} \rangle$ and $\langle P_{e,t} \rangle$, resulting in no change in the flow. That is, in the case of no drag reduction, the following relation should be valid:

$$\begin{aligned} \langle P_{e,m} \rangle &= (1-\beta) \cdot \langle \epsilon_m \rangle_{Newtonian} - (1-\beta) \cdot \left\langle \frac{1}{Re} \frac{d^2 k_m}{dy^2} \right\rangle_{Newtonian}, \\ \langle P_{e,t} \rangle &= (1-\beta) \cdot \langle \epsilon_k \rangle_{Newtonian} - (1-\beta) \cdot \left\langle \frac{1}{Re} \frac{d^2 k_t}{dy^2} \right\rangle_{Newtonian}. \end{aligned} \tag{4.8}$$

Then, substituting (4.8) into (4.5) and (4.6), one can clearly see that the dynamic equations for the mean and turbulent kinetic energy become the same as those for the Newtonian fluid flow. In figure 11, solid lines are drawn to denote the magnitudes of $(1-\beta)$ times the dissipations of the mean and turbulent kinetic energy, and their sum for the Newtonian fluid flow, which clearly shows the validity of (4.8) in the case of no drag reduction because the magnitude of the second term in the right hand side of (4.8) is much smaller than that of the first term. However, when drag reduction occurs (for example, at $We = 3$ and 1 at $Re = 3000$ and 15000, respectively), the energy transfer becomes quite intermittent and more energy is transferred from the flow to the polymer, as shown in figure 10 .

In order to investigate the detailed feature about the energy transfer, the spatial distributions of $P_{e,m}$, $P_{e,t}$ and $-k_e/We$ are shown in figure 12. It is seen that the polymer stores and releases most of energy near the wall. Although the amounts of the production and dissipation of the elastic energy increase globally with increasing We (figure 10), they decrease locally very near the wall ($y^+ \leqslant 10$) but increase in the buffer and log layers. Interestingly, the same feature was observed in u_{rms} (figure 3), so was in the turbulent kinetic energy. Thus, we conjecture that, when drag reduction occurs, the polymer takes less energy from the flow in the very near-wall region and returns more energy to the flow in the buffer and log layers, and also that the polymer transports its elastic energy stored in the very near-wall region to the flow in the buffer and log layers.

This conjecture can be verified from the probability density function (PDF) of the elastic-energy production. The PDFs of $P_{e,m}$ and $P_{e,t}$ are shown in figure 13. Negative values of $P_{e,m}$ and $P_{e,t}$ represent the transport of the elastic energy of the polymer to the mean and turbulent kinetic energy of the flow, respectively. The probabilities of having negative $P_{e,m}$ and $P_{e,t}$ are shown in table 2. The energy transfer from the elastic energy

Re	We	$DR(\%)$	$P_{e,m}$		$P_{e,t}$	
			$y_0^+ \simeq 5$	$y_0^+ \simeq 30$	$y_0^+ \simeq 5$	$y_0^+ \simeq 30$
3000	1	0	0%	21%	49%	3%
	3	20	0%	18%	57%	31%

TABLE 2. Probabilities of negative $P_{e,m}$ and $P_{e,t}$ ($\int \mathrm{PDF}(P_{e,m} < 0)dP_{e,m}$ and $\int \mathrm{PDF}(P_{e,t} < 0)dP_{e,t}$) in percentage.

to the mean kinetic energy (i.e. $P_{e,m} < 0$) at either $y_0^+ \simeq 5$ or 30 is nearly unchanged with respect to the Weissenberg number. However, a significant change occurs in the energy transfer from the elastic energy to the turbulent kinetic energy (i.e. $P_{e,m} < 0$) at $y_0^+ \simeq 30$ when drag reduction occurs. That is, this energy transfer significantly increases at $y_0^+ \simeq 30$ (from 3% at $We = 1$ to 31% at $We = 3$), indicating that, in the case of drag reduction, the polymer returns energy to the flow in the buffer layer much more than in the case of no drag reduction.

In order to see that the near-wall elastic energy is transported to the buffer and log layers, the time sequence of the elastic energy k_p in a coordinate moving with the structures is shown in figure 14 for the cases with and without drag reduction at $Re = 3000$. In the case of no drag reduction ($We = 1$), high elastic energy exists only very near the wall. However, when drag reduction occurs ($We = 3$), high elastic energy existing very near the wall is transported to the buffer and log layers even though the cross-plane velocity fluctuations are much weaker than those for $We = 1$. A similar behaviour was also observed for $Re = 15000$.

The relaxation time of the polymer solution is essentially associated with the transport of the elastic energy. Fluid particles containing high elastic energy very near the wall are lifted away from the wall by the near-wall vortical motion (see figure 15). When the relaxation time is short (i.e. low We), the particles release the elastic energy very near the

wall before they reach the buffer layer. When the relaxation time is long enough, however, the elastic energy absorbed from the kinetic energy is delivered to the buffer and log layers and released there, which results in weakening of near-wall turbulence (see also figure 3). Massah & Hanratty (1997) showed that the polymer chains are stretched in the very near-wall region (meaning that the polymer absorbs high elastic energy) and released in the buffer and log layers, supporting the present drag reduction mechanism. The dynamic sequence described in figure 15 also explains the intermittent energy transport behavior shown in figure 10 in the case of drag reduction.

5. Conclusions and further remarks

In the present study, direct numerical simulation of turbulent viscoelastic flow in a channel was conducted to investigate the drag reduction mechanism by polymer additives. An Oldroyd-B model was used for the constitutive equation for the polymer stress to represent the viscoelastic nature of the polymer. The simulations were carried out by changing the Weissenberg number at the bulk Reynolds numbers of 4000 and 20000.

The onset criterion for drag reduction predicted in the present study was in good agreement with previous theoretical and experimental studies. The flow statistics such as the mean velocity, turbulence intensities and Reynolds shear stress were also in good agreements with those in the previous experimental studies. In addition, the stress deficit that shows the role of the elasticity on drag reduction was observed.

The transport equations for the mean and turbulent kinetic energy and elastic energy were derived from the kinetic and elastic theory and were investigated. From the probability density functions of the production terms in those transport equations and also from the time sequence of the polymer elastic energy, we obtained the following mechanism for drag reduction by polymer additives. When drag reduction occurs, the

turbulent kinetic energy near the wall is absorbed by polymer and transformed to the elastic energy. Then, the elastic energy obtained near the wall is lifted up by the near-wall vortical motion and released into the turbulent kinetic energy or is dissipated in the buffer and log layers. Thus, the polymer actively intervenes into the energy transfer. Therefore, in order to obtain drag reduction, the relaxation time of polymer should be long enough to transport the elastic energy from the near-wall region to the buffer or log layer. Otherwise, the elastic energy obtained near the wall is released there and the equilibrium state exists in terms of energy exchange, resulting in no drag change.

The drag-reduction mechanism proposed here in terms of the elastic theory does not imply that the mechanism explained using the extensional viscosity is incorrect, as Sreenivasan & White (2000) mentioned. It is because any reasonable viscoelastic model (such as the FENE-P model or the Oldroyd-B model) suggests that an elastic effect can be formally interpreted in terms of an extensional viscosity effect, despite the fundamental difference between the two mechanisms. However, when the extensional viscosity alone is considered for polymer drag reduction, as done by Orlandi (1995) and den Toonder *et al.* (1997), the question why the onset of drag reduction exists is very difficult to answer, which is the main reason that the elastic theory is introduced in the present study. After the onset, on the other hand, it is still premature to clearly identify which of the two mechanisms is dominant for drag reduction, because the behavior of turbulence in the presence of polymer is still largely unknown. Especially, the interaction between the polymer and the near-wall streamwise vortices should be an important research subject to be investigated in the future.

Finally, it is certainly important to investigate the flow field with non-homogeneous polymer concentration especially in the wall-normal direction, which is very difficult to obtain physically meaningful results from the present approach. However, the present

drag reduction mechanism suggests that the high concentration of polymer between the viscous sublayer and buffer layer should decrease drag significantly.

This study was supported by the Creative Research Initiatives and Korea Institute of Science & Technology Evaluation Planning (No. I-01-03-A-024) of the Korean Ministry of Science and Technology.

Appendix. Examination of unboundedness of polymer stretch in the Oldroyd-B model

Theoretically, the polymer stretch in the Oldroyd-B model is not upper bounded. However, in a real flow field, it may not be the case because the time evolution of the polymer stretch is coupled with that of the shear rate. The FENE-P model becomes the Oldroyd-B model as $L^2 \to \infty$ (Bird *et al.* 1987), where L^2 is the dumbbell extensibility of the FENE-P model. Thus, the Oldroyd-B model is a limiting case of the FENE-P model, and the FENE-P model behaves like the Oldroyd-B model when L^2 is sufficiently large.

In order to compare the magnitudes of the polymer stretch from both the FENE-P and Oldroyd-B models for the present flow, a computer code developed by Min *et al.* (2001) is used for the simulation with the FENE-P model. Figure 16 shows the time histories of the polymer stretch c_{kk} at $y_0^+ = 0.2$ and $y_0^+ = 10$. One can clearly see that the c_{kk} of the Oldroyd-B model is upper bounded in the present flow, and the boundedness of the FENE-P model with $L^2 = 3600$ is almost the same as that of the Oldroyd-B model. This value of L^2 corresponds roughly to a polystyrene molecule of 10^6 molecular weight (Dubief & Lele 2001). This figure also suggests that the FENE-P model with $L^2 = 1000$, adopted by Ptasinski *et al.* (2002), shows a similar behavior to that of the Oldroyd-B model. Figures 17 (a) and (b) show the time histories of the mean pressure gradient and

the rms velocity fluctuations at $Re = 3000$ and $We = 2$, respectively. One can again see that the results of the Oldroyd-B model are in good agreements with those of the FENE-P model with $L^2 = 3600$.

REFERENCES

Berman, N. S. 1977 Flow time scales and drag reduction. *Phys. Fluids* **20**, s168–s174.

Bird, R. B., Curtiss, C. F., Armstrong, R. C. & Hassager, O. 1987 *Dynamics of polymeric liquids*, vol. 2, Kinetic Theory. John Wiley & Sons.

Cadot, O., Bonn, D. & Douady, S. 1998 Turbulent drag reduction in a closed flow system: Boundary layer versus bulk effects. *Phys. Fluids* **10**, 426–436.

Choi, H., Moin, P. and Kim, J. 1992 Turbulent drag reduction: studies of feedback control and flow over riblets. *Rep.* TF-55. Department of Mechanical Engineering, Stanford University, Stanford, CA.

Choi, H., Moin, P. and Kim, J. 1993 Direct numerical simulation of turbulent flow over riblets. *J. Fluid Mech.* **255**, 503–539.

Choi, H., Moin, P. and Kim, J. 1994 Active turbulence control for drag reduction in wall-bounded flows. *J. Fluid Mech.* **262**, 75–110.

De Gennes, P. G. 1990 *Introduction to Polymer Dynamics.* Cambridge University Press.

Den Toonder, J. M. J., Hulsen, M. A., Kuiken, G. D. C. & Nieuwstadt, F. T. M. 1997 Drag reduction by polymer additives in a turbulent pipe flow: numerical and laboratory experiments. *J. Fluid Mech.* **337**, 193–231.

Dimitropoulos, C. D., Sureshkumar, R. & Beris, A. N. 1998 Direct numerical simulation of viscoelastic turbulent channel flow exhibiting drag reduction: effect of the variation of rheological parameters. *J. Non-Newtonian Fluid Mech.* **79**, 433–468.

Dubief, Y. & Lele, S. K. 2001 Direct numerical simulation of polymer flow. *Center for Turbulence Research Annual Briefs 2001.* 197–208.

Goldshtik, M. A., Zametalin, V. V. & Shtern, V. N. 1982 Simplified theory of the near-wall turbulent layer of Newtonian and drag-reducing fluids. *J. Fluid Mech.* **119**, 423–441.

Gyr, A & Tsinober, A. 1997 On the rheological nature of drag reduction phenomena. *J. Non-Newtonian Fluid Mech.* **73**, 153–162.

Hershey, H. C. & Zakin, J. L. 1967 A molecular approach to predicting the onset of drag reduction in the turbulent flow of dilute polymer solutions. *Chem. Eng. Sci.* **22**, 1847–1856.

Hinch, E. J. 1977 Mechanical models of dilute polymer solutions in strong flows. *Phys. Fluids* **20**, s22–s30.

Jiménez, J. & Moin, P. 1991 The minimal flow unit in near-wall turbulence. *J. Fluid. Mech.* **225**, 213–240.

Joseph, D. D. 1990 *Fluid Dynamics of Viscoelastic Liquids.* Springer-Verlag.

Joseph, D. D. & Christodoulou, C. 1993 Independent confirmation that delayed die swell is a hyperbolic transition. *J. Non-Newtonian Fluid. Mech.* **48**, 225–235.

Lee, D. & Choi, H. 2001 MHD turbulent flow in a channel at low magnetic Reynolds number. *J. Fluid. Mech.* **439**, 367–394.

Lele, S. K. 1992 Compact finite difference schemes with spectral-like resolution. *J. Comput. Phys.* **103**, 16–42.

Lumley, J. L. 1969 Drag reduction by additives. *Ann. Rev. Fluid Mech.* **1**, 367–384.

Lumley, J. L. 1973 Drag reduction in turbulent flow by polymer additives. *J. Polymer Sci., Macromol. Rev.* **7**, 263–290.

Luchik, T. S. & Tiederman, W. G. 1988 Turbulent structure in low-concentration drag-reducing channel flows. *J. Fluid Mech.* **190**, 241–263.

Massah, H. & Hanratty, T. J. 1997 Added stresses because of the presence of FENE-P bead-spring chains in a random velocity field. *J. Fluid Mech.* **337**, 67–101.

Min, T., Choi, H. & Yoo, J. Y. 2002 Maximum drag reduction in a turbulent channel flow by polymer additives. *Proc. 55th Annual Meeting of APS DFD*, 53.

Min, T., Yoo, J. Y. & Choi, H. 2001 Effect of spatial discretization schemes on numerical solutions of viscoelastic fluid flows. *J. Non-Newtonian Fluid Mech* **100**, 27–47.

Moser, R. D., Kim, J. & Mansour, N. N. 1999 Direct numerical simulation of turbulent channel flow up to $Re_\tau = 590$. *Phys. Fluids.* **11**, 943–945.

Orlandi, P. 1995 A tentative approach to the direct simulation of drag reduction by polymers. *J. Non-Newtonian Fluid Mech.* **60**, 277–301.

Pincus, P. 1976 Excluded volume effects and stretched polymer-chains. *Macromolecules* **9**, 386–388.

Ptasinki, P. K., Boersma, B. J., Nieuwstadt, F. T. M., van der Brule, B. H. A. A. & Hunt, J. C. R. 2002 Turbulent channel flow near maximum drag reduction: simulations, experiments and mechanisms. Submitted for publication.

Smith, D. E. & Chu, S. 1998 Response of flexible polymers to a sudden elongational flow. *Science* **281**, 1335-1340.

Sreenivasan, K. R. & White, C. M. 2000 The onset of drag reduction by dilute polymer additives, and the maximum drag reduction asymptote. *J. Fluid Mech.* **409**, 149–164.

Sureshkumar, R., Beris, A. N. & Handler, R. A. 1997 Direct numerical simulation of the turbulent channel flow of a polymer solution. *Phys. Fluids.* **9**, 743–755.

Tabor, M. & de Gennes, P. G. 1986 A cascade theory of drag reduction. *Europhys. Lett.* **2**, 519–522.

Tolstykh, A. I. & Lipavskii, M. V. 1998 On performance of methods with third- and fifth-order compact upwind differencing. *J. Comput. Phys.* **140**, 205–232.

Toms, B. A. 1949 Some observations on the flow of linear polymer solutions through straight tubes at large Reynolds numbers. *Proc. 1st International Congress on Rheology.* **2**, 135–141.

Tulin, M. P. 1966 Hydrodynamic aspects of macromolecular solutions. *Proc. 6th Symposium on Naval Hydrodynamics.* 3–18.

Virk, P. S. 1971 An elastic sublayer model for drag reduction by dilute solutions of linear macromolecules. *J. Fluid Mech.* **45**, 417–440.

Virk, P. S., Merril, E. W., Mickley, H. S., Smith, K. A. & Mollo-Christensen, E. L. 1967 The Toms phenomenon-turbulent pipe flow of dilute polymer solutions. *J. Fluid Mech.* **30**, 305–328.

Warholic, M. D., Massah, H. and Hanratty, T. J. 1999 Influence of drag-reducing polymers on turbulence: effects of Reynolds number, concentration and mixing. *Exp. Fluids* **27**, 461–472.

Wei, T. & Willmarth, W. W. 1992 Modifying turbulent structure with drag-reducing polymer additives in turbulent channel flows. *J. Fluid Mech.* **245**, 619–641.

List of Figures

1 Time histories of the mean pressure gradient normalized by that of Newtonian fluid flow: (a) $Re = 3000$ (——, Newtonian; ····· with •, $We = 0.1$; $-\cdot-\cdot-$ with •, $We = 0.5$; $---$, $We = 1$; $-\cdot-\cdot-$, $We = 2$; ·····, $We = 3$; $-\cdot\cdot-\cdot\cdot-$, $We = 4$); (b) $Re = 15000$ (——, Newtonian; ····· with •, $We = 0.2$; $---$, $We = 0.3$; $-\cdot-\cdot-$, $We = 0.5$; ·····, $We = 1$; $-\cdot\cdot-\cdot\cdot-$, $We = 2$). 31

2 Mean streamwise velocities normalized by actual wall-shear velocity u_τ: (a) $Re = 3000$ (——, Newtonian; $---$, $We = 1$; $-\cdot-\cdot-$, $We = 2$; ·····, $We = 3$; $-\cdot\cdot-\cdot\cdot-$, $We = 4$); (b) $Re = 15000$ (——, Newtonian; $---$, $We = 1$; ·····, $We = 2$). Also shown are the experimental results from Luchik & Tiederman (1988; □, Newtonian; △, polymer) and Wei & Willmarth (1992; ◯, Newtonian; ◊, polymer). 32

3 Root-mean-square velocity fluctuations normalized by the wall-shear velocity u_{τ_0}: (a) $Re = 3000$; (b) $Re = 15000$. Lines and symbols are the same as those in figure 2. Here, $y_0^+ = yu_{\tau_0}/\nu$. 33

4 Root-mean-square vorticity fluctuations normalized by the wall-shear velocity u_{τ_0}: (a) $Re = 3000$; (b) $Re = 15000$. Lines are the same as those in figure 2. Lines with ■ denote ω_x, lines ω_y and lines with • ω_z, respectively. 34

5 Reynolds shear stresses and total shear stresses normalized by the wall-shear velocity u_{τ_0}: (a) $Re = 3000$; (b) $Re = 15000$. Lines and symbols for the Reynolds shear stress are the same as those in figure 2. Lines with • denote the total shear stress. 35

6 Stress deficits normalized by the actual wall-shear velocity u_τ: (a) $Re = 3000$; (b) $Re = 15000$. Lines are the same as those in figure 2. 36

7 Power spectra of the polymer stresses normalized by $u_{\tau_0}^2$ at $Re = 3000$: (a) $y_0^+ \simeq 10$; (b) $y_0^+ \simeq 30$. For $We = 1$ (no drag reduction), ——, $(1-\beta)/Re \cdot \tau_{11}$; − − −, $(1-\beta)/Re \cdot \tau_{22}$; ·····, $(1-\beta)/Re \cdot \tau_{33}$; for $We = 3$ (20% drag reduction), •, $(1-\beta)/Re \cdot \tau_{11}$; ▲, $(1-\beta)/Re \cdot \tau_{22}$; ■, $(1-\beta)/Re \cdot \tau_{33}$. 37

8 Time histories of the volume-averaged production $\langle P_k \rangle$ and dissipation $\langle \epsilon_k \rangle$ of the turbulent kinetic energy normalized by $u_{\tau_0}^3/\delta$: (a) $Re = 3000$; (b) $Re = 15000$. The lines are the same as those in figure 1. 38

9 Profiles of the production P_k and dissipation ϵ_k of the turbulent kinetic energy normalized by $u_{\tau_0}^3/\delta$: (a) $Re = 3000$; (b) $Re = 15000$. The lines are the same as those in figure 1. 39

10 Time histories of the volume-averaged productions, $\langle P_{e,m} \rangle$ and $\langle P_{e,t} \rangle$, and dissipation, $-\langle k_e \rangle / We$, of the elastic energy normalized by $u_{\tau_0}^3/\delta$: (a) $Re = 3000$ (− − −, $We = 1$; ·····, $We = 3$); (b) $Re = 15000$ (− − −, $We = 0.3$; ·····, $We = 1$). 40

11 Time histories of the volume-averaged productions, $\langle P_{e,m} \rangle$ and $\langle P_{e,t} \rangle$, and dissipation, $-\langle k_e \rangle / We$, of the elastic energy normalized by $u_{\tau_0}^3/\delta$ ($Re = 3000$): − ·· − ·· −, $We = 0.1$; − · − · −, $We = 0.5$; − − −, $We = 1$. Solid lines in this figure denote the magnitudes of $(1-\beta)$ times the dissipations of the mean and turbulent kinetic energy, and their sum for the Newtonian fluid flow. 41

12 Profiles of the productions, $P_{e,m}$ and $P_{e,t}$, and dissipation, $-k_e/We$, of the elastic energy normalized by $u_{\tau_0}^3/\delta$: (a) $Re = 3000$ (− − −, $We = 1$; ·····, $We = 3$); (b) $Re = 15000$ (− − −, $We = 0.3$; ·····, $We = 1$). 42

13 Probability density functions of $P_{e,m}$ and $P_{e,t}$ normalized by $u_{\tau_0}^3/\delta$ at $Re = 3000$: (a) $P_{e,m}$; (b) $P_{e,t}$. 43

14 Time sequence of the instantaneous elastic energy k_p normalized by $u_{\tau_0}^2$ in a coordinate moving with the structures at $Re = 3000$: (a) $We = 1$; (b) $We = 3$. The time interval between the consecutive instants is 0.2. 44

15 Schematic representation of the present drag reduction mechanism. 45

16 Time histories of the polymer stretch c_{kk} at $Re = 3000$ and $We = 2$: (a) $y_0^+ = 0.2$; (b) $y_0^+ = 10$. ——, FENE-P model with $L^2 = 3600$; ·····, Oldroyd-B model. 46

17 Comparison of the results from the Oldroyd-B and FENE-P models at $Re = 3000$ and $We = 2$: (a) time histories of the mean pressure gradient normalized by that of Newtonian fluid flow; (b) root-mean-square velocity fluctuations normalized by the wall-shear velocity u_{τ_0}. ——, Newtonian; – – –, Oldroyd-B model; ·····, FENE-P model with $L^2 = 3600$. 47

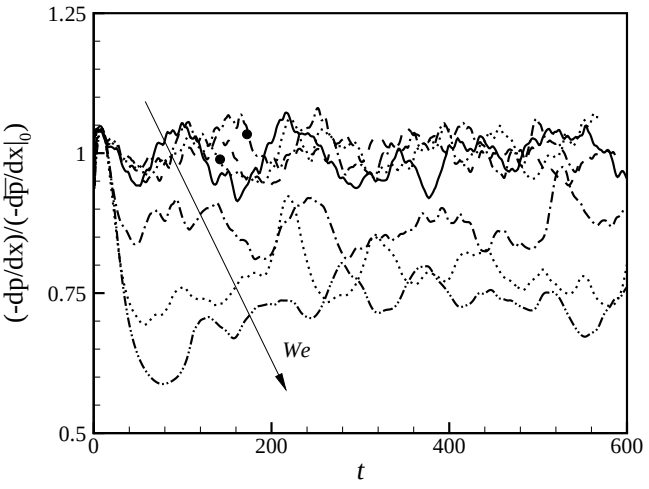

(a)

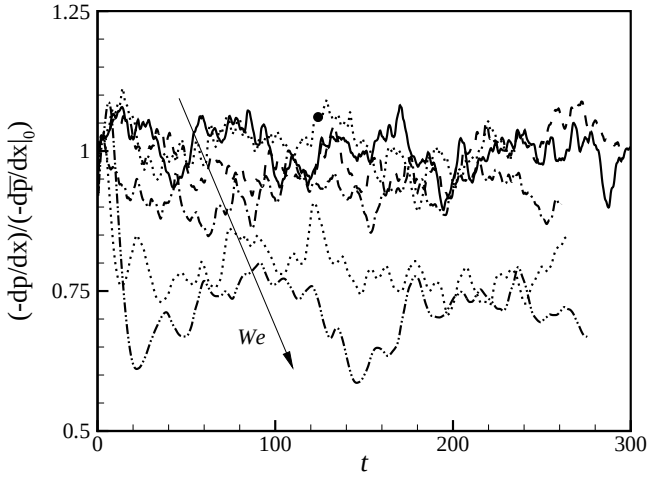

(b)

FIGURE 1. Time histories of the mean pressure gradient normalized by that of Newtonian fluid flow: (a) $Re = 3000$ (——, Newtonian; ····· with •, $We = 0.1$; $-\cdot-\cdot-$ with •, $We = 0.5$; $--$, $We = 1$; $-\cdot-\cdot-$, $We = 2$; ·····, $We = 3$; $-\cdot\cdot-\cdot\cdot-$, $We = 4$); (b) $Re = 15000$ (——, Newtonian; ····· with •, $We = 0.2$; $--$, $We = 0.3$; $-\cdot-\cdot-$, $We = 0.5$; ·····, $We = 1$; $-\cdot\cdot-\cdot\cdot-$, $We = 2$).

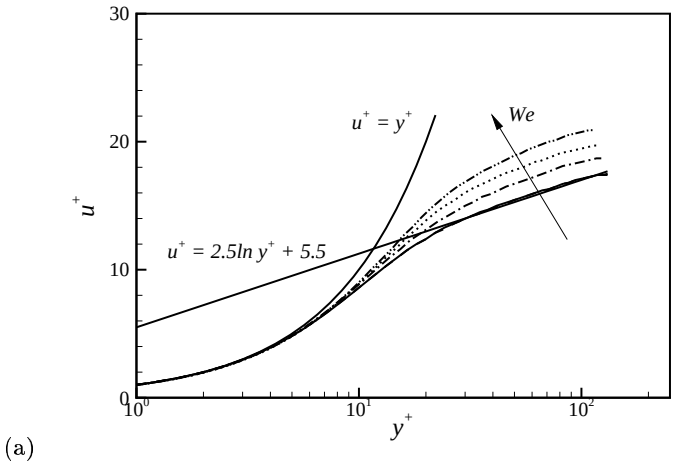

(a)

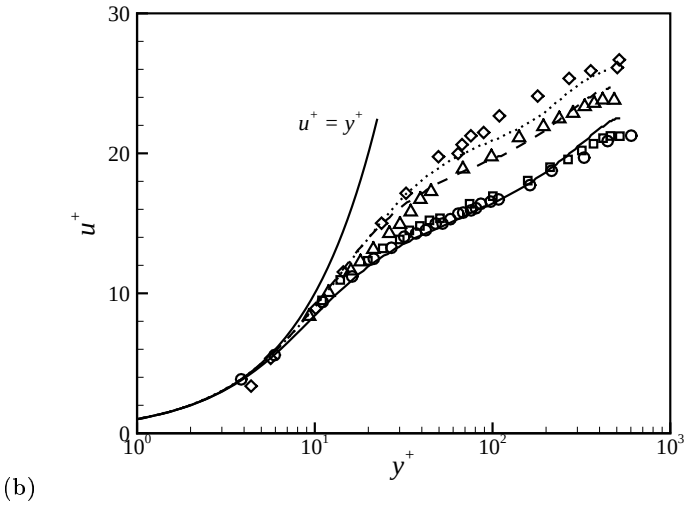

(b)

FIGURE 2. Mean streamwise velocities normalized by actual wall-shear velocity u_τ: (a) $Re = 3000$ (——, Newtonian; − − −, $We = 1$; − · − · −, $We = 2$; ·····, $We = 3$; − ·· − ·· −, $We = 4$); (b) $Re = 15000$ (——, Newtonian; − − −, $We = 1$; ·····, $We = 2$). Also shown are the experimental results from Luchik & Tiederman (1988; □, Newtonian; △, polymer) and Wei & Willmarth (1992; ◯, Newtonian; ◊, polymer).

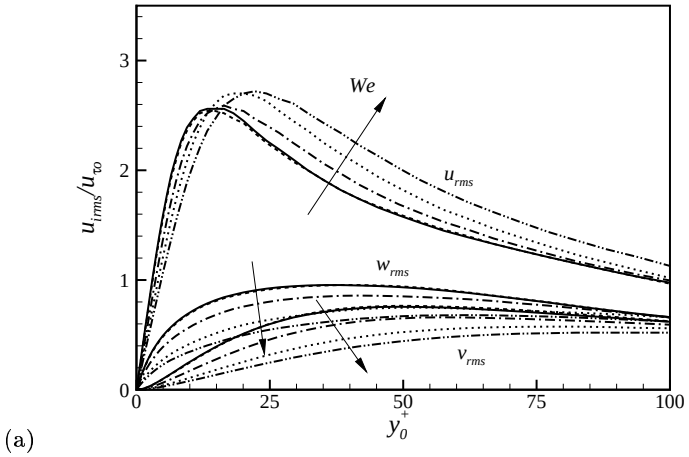

(a)

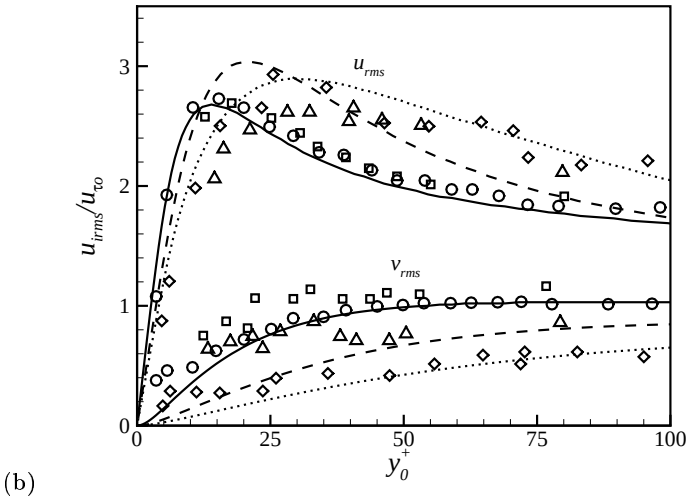

(b)

FIGURE 3. Root-mean-square velocity fluctuations normalized by the wall-shear velocity u_{τ_0}: (a) $Re = 3000$; (b) $Re = 15000$. Lines and symbols are the same as those in figure 2. Here, $y_0^+ = y u_{\tau_0}/\nu$.

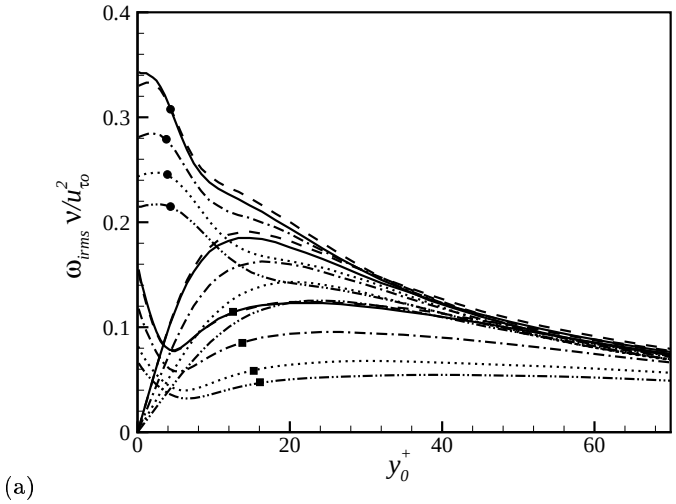

(a)

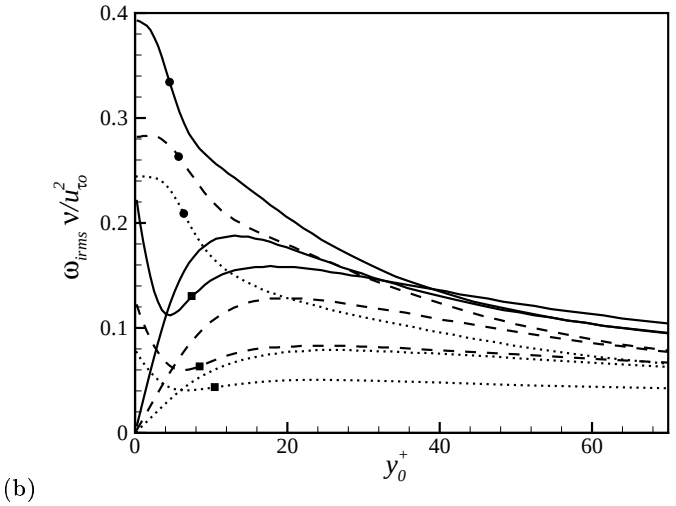

(b)

FIGURE 4. Root-mean-square vorticity fluctuations normalized by the wall-shear velocity u_{τ_0}: (a) $Re = 3000$; (b) $Re = 15000$. Lines are the same as those in figure 2. Lines with ■ denote ω_x, lines ω_y and lines with • ω_z, respectively.

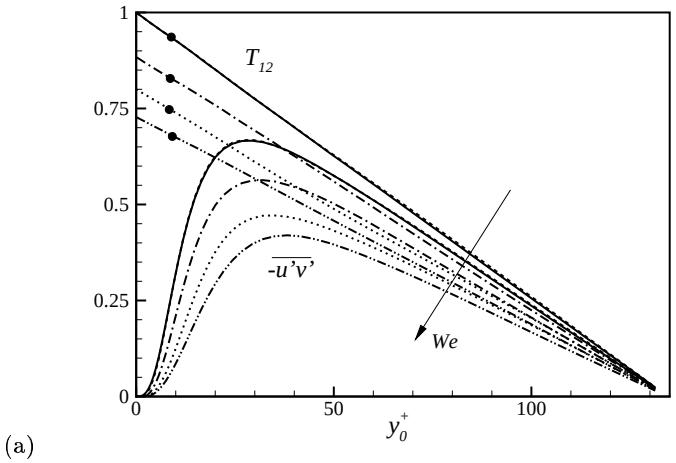

(a)

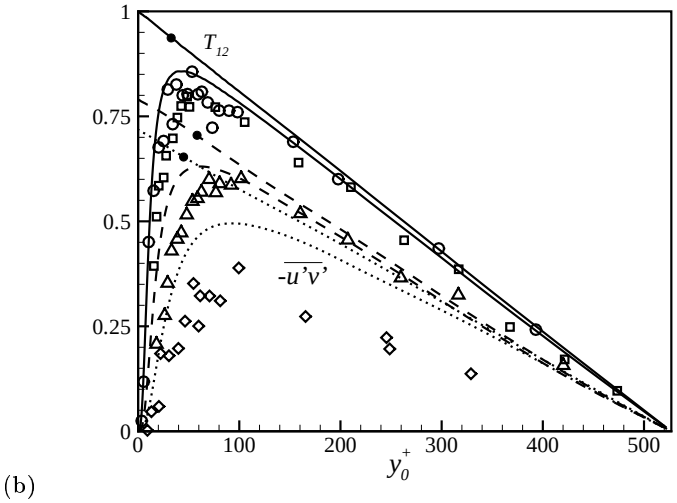

(b)

FIGURE 5. Reynolds shear stresses and total shear stresses normalized by the wall-shear velocity u_{τ_0}: (a) $Re = 3000$; (b) $Re = 15000$. Lines and symbols for the Reynolds shear stress are the same as those in figure 2. Lines with • denote the total shear stress.

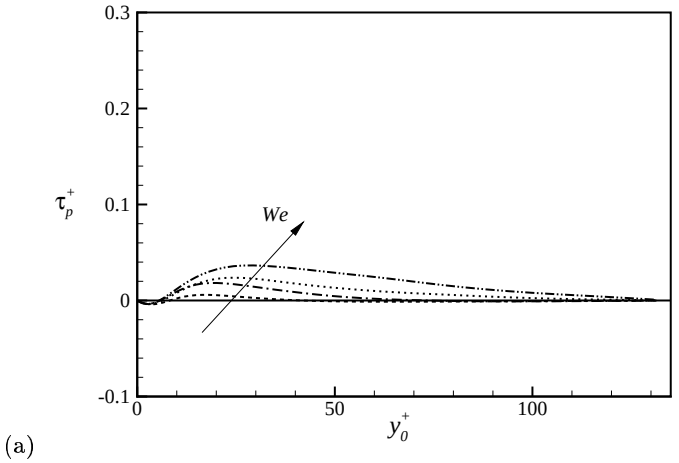

(a)

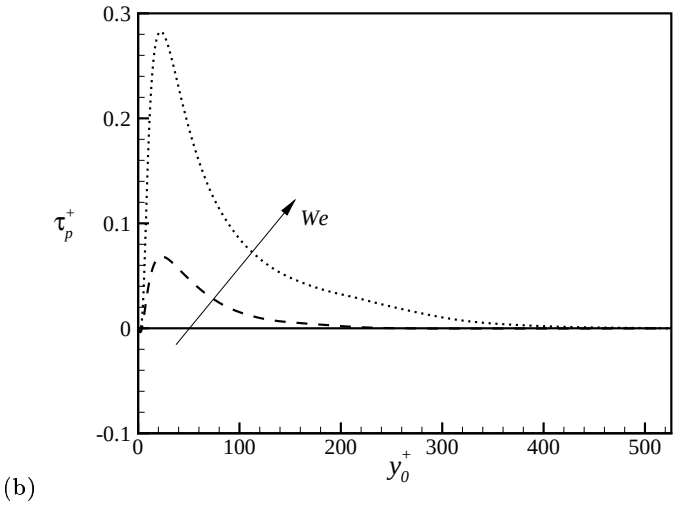

(b)

FIGURE 6. Stress deficits normalized by the actual wall-shear velocity u_τ: (a) $Re = 3000$; (b) $Re = 15000$. Lines are the same as those in figure 2.

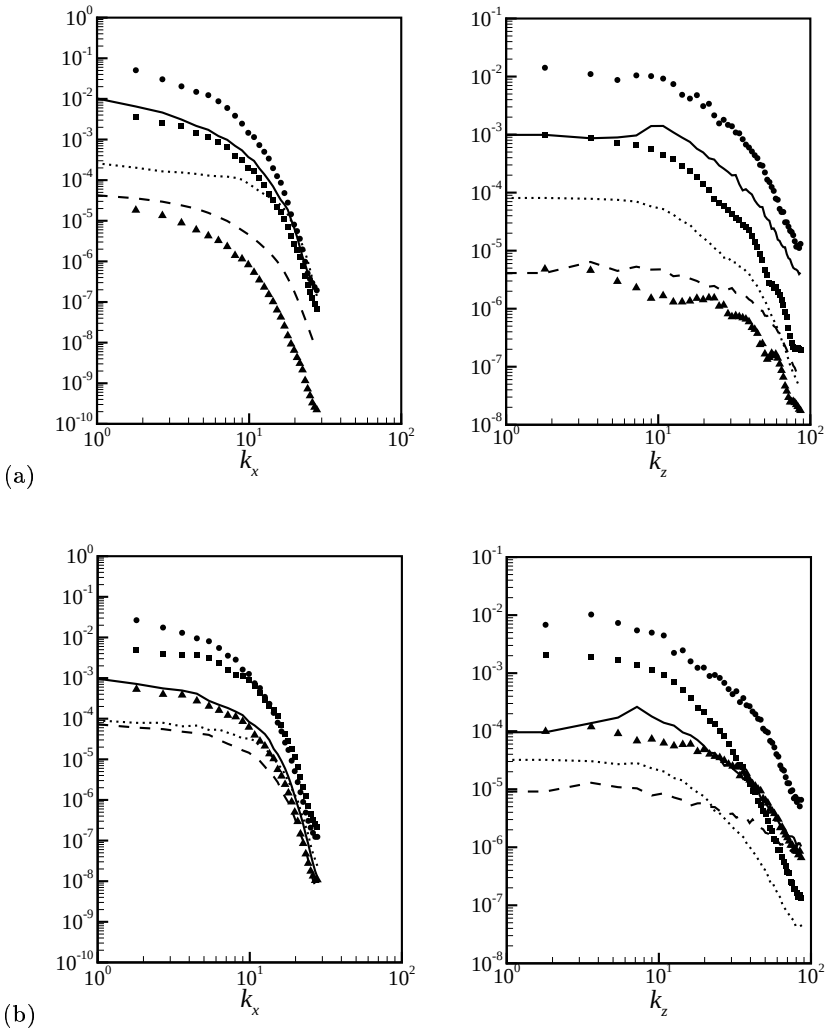

FIGURE 7. Power spectra of the polymer stresses normalized by $u_{\tau_0}^2$ at $Re = 3000$: (a) $y_0^+ \simeq 10$; (b) $y_0^+ \simeq 30$. For $We = 1$ (no drag reduction), ——, $(1-\beta)/Re \cdot \tau_{11}$; – – –, $(1-\beta)/Re \cdot \tau_{22}$; ·····, $(1-\beta)/Re \cdot \tau_{33}$; for $We = 3$ (20% drag reduction), •, $(1-\beta)/Re \cdot \tau_{11}$; ▲, $(1-\beta)/Re \cdot \tau_{22}$; ■, $(1-\beta)/Re \cdot \tau_{33}$.

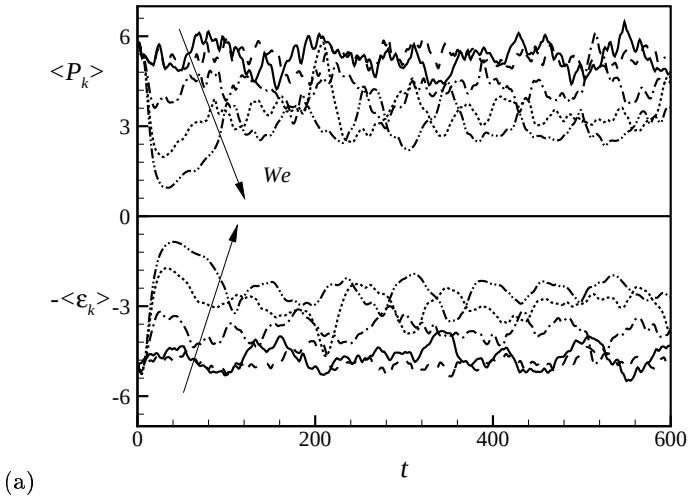

(a)

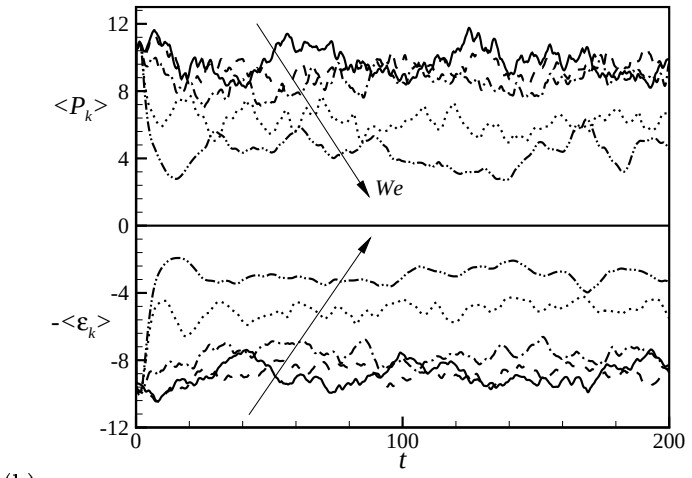

(b)

FIGURE 8. Time histories of the volume-averaged production $\langle P_k \rangle$ and dissipation $\langle \epsilon_k \rangle$ of the turbulent kinetic energy normalized by $u_{\tau_0}^3/\delta$: (a) $Re = 3000$; (b) $Re = 15000$. The lines are the same as those in figure 1.

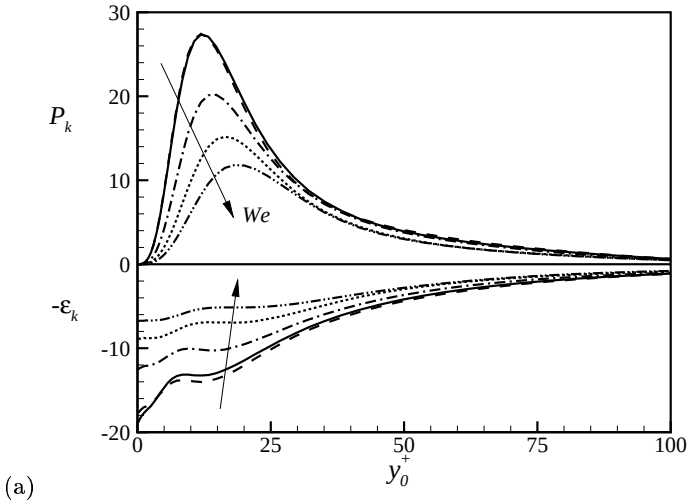

(a)

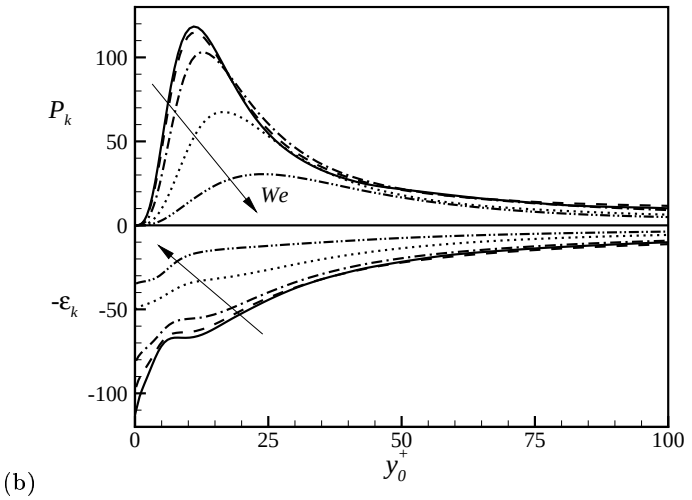

(b)

FIGURE 9. Profiles of the production P_k and dissipation ϵ_k of the turbulent kinetic energy normalized by $u_{\tau_0}^3/\delta$: (a) $Re = 3000$; (b) $Re = 15000$. The lines are the same as those in figure 1.

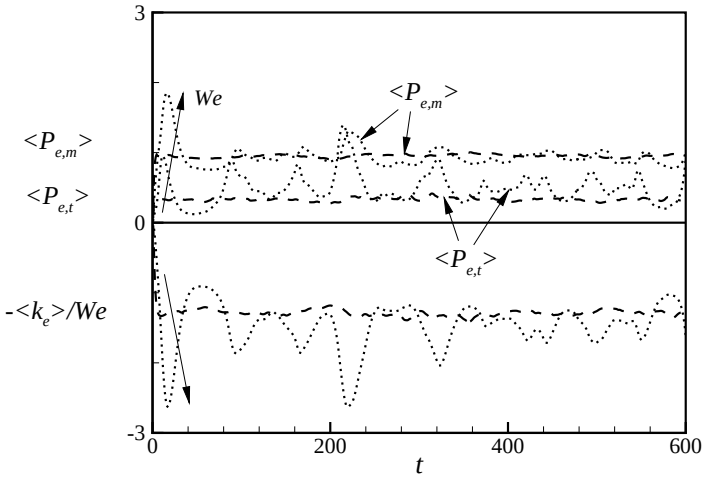

(a)

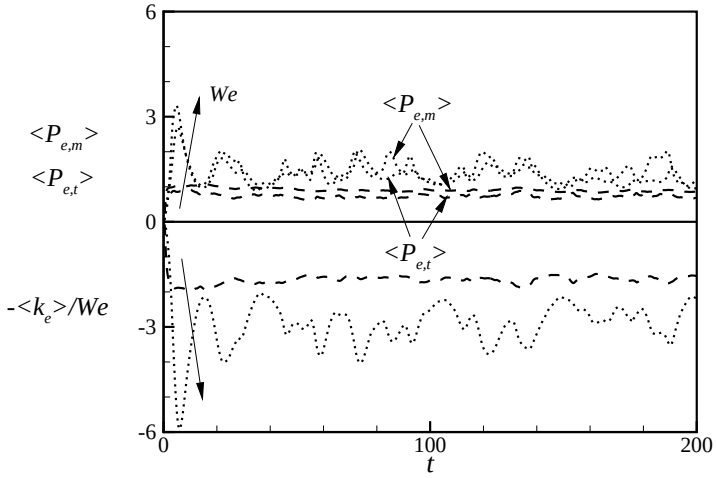

(b)

FIGURE 10. Time histories of the volume-averaged productions, $\langle P_{e,m} \rangle$ and $\langle P_{e,t} \rangle$, and dissipation, $-\langle k_e \rangle / We$, of the elastic energy normalized by $u_{\tau_0}^3/\delta$: (a) $Re = 3000$ ($---$, $We = 1$; $\cdots\cdots$, $We = 3$); (b) $Re = 15000$ ($---$, $We = 0.3$; $\cdots\cdots$, $We = 1$).

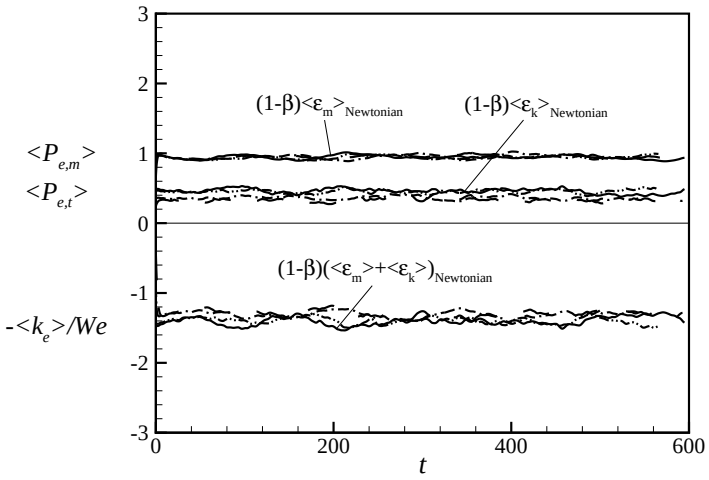

FIGURE 11. Time histories of the volume-averaged productions, $\langle P_{e,m} \rangle$ and $\langle P_{e,t} \rangle$, and dissipation, $-\langle k_e \rangle / We$, of the elastic energy normalized by $u_{\tau_0}^3/\delta$ ($Re = 3000$): $-\cdot\cdot-\cdot\cdot-$, $We = 0.1$; $-\cdot-\cdot-$, $We = 0.5$; $---$, $We = 1$. Solid lines in this figure denote the magnitudes of $(1-\beta)$ times the dissipations of the mean and turbulent kinetic energy, and their sum for the Newtonian fluid flow.

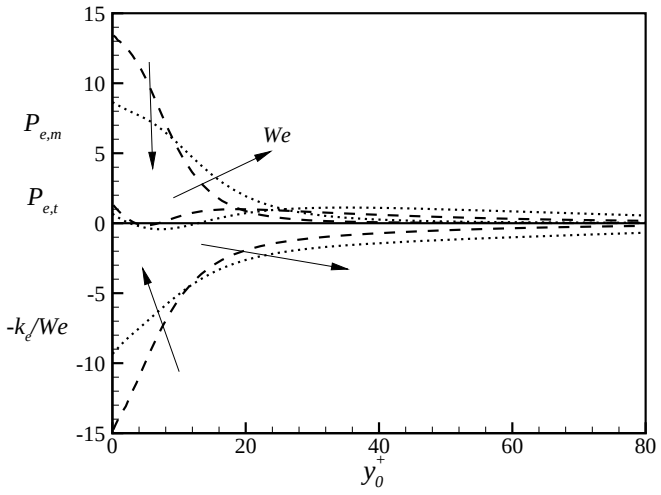

(a)

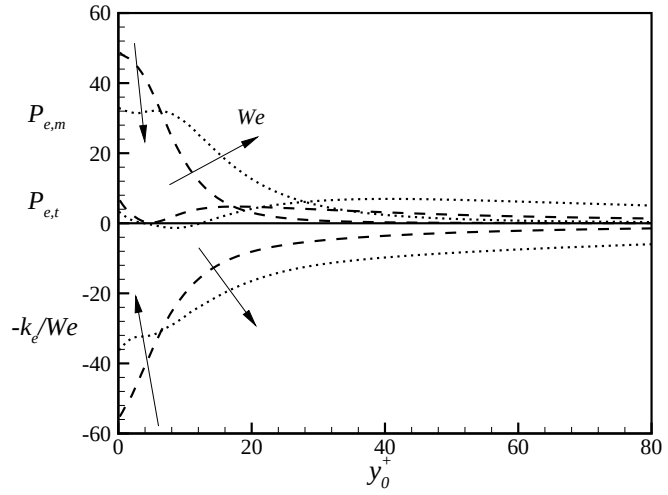

(b)

FIGURE 12. Profiles of the productions, $P_{e,m}$ and $P_{e,t}$, and dissipation, $-k_e/We$, of the elastic energy normalized by $u_{\tau_0}^3/\delta$: (a) $Re = 3000$ (– – –, $We = 1$; ·····, $We = 3$); (b) $Re = 15000$ (– – –, $We = 0.3$; ·····, $We = 1$).

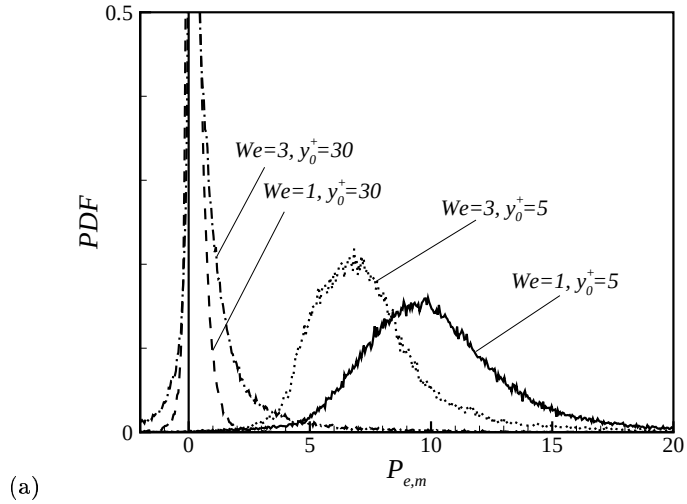

(a)

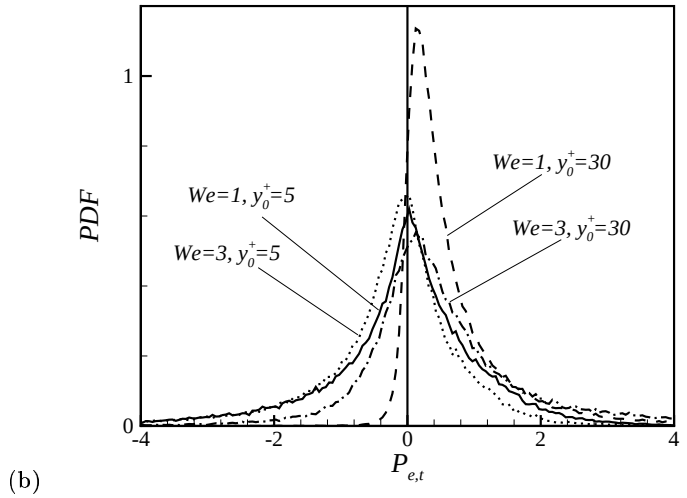

(b)

FIGURE 13. Probability density functions of $P_{e,m}$ and $P_{e,t}$ normalized by $u_{\tau_0}^3/\delta$ at $Re = 3000$: (a) $P_{e,m}$; (b) $P_{e,t}$.

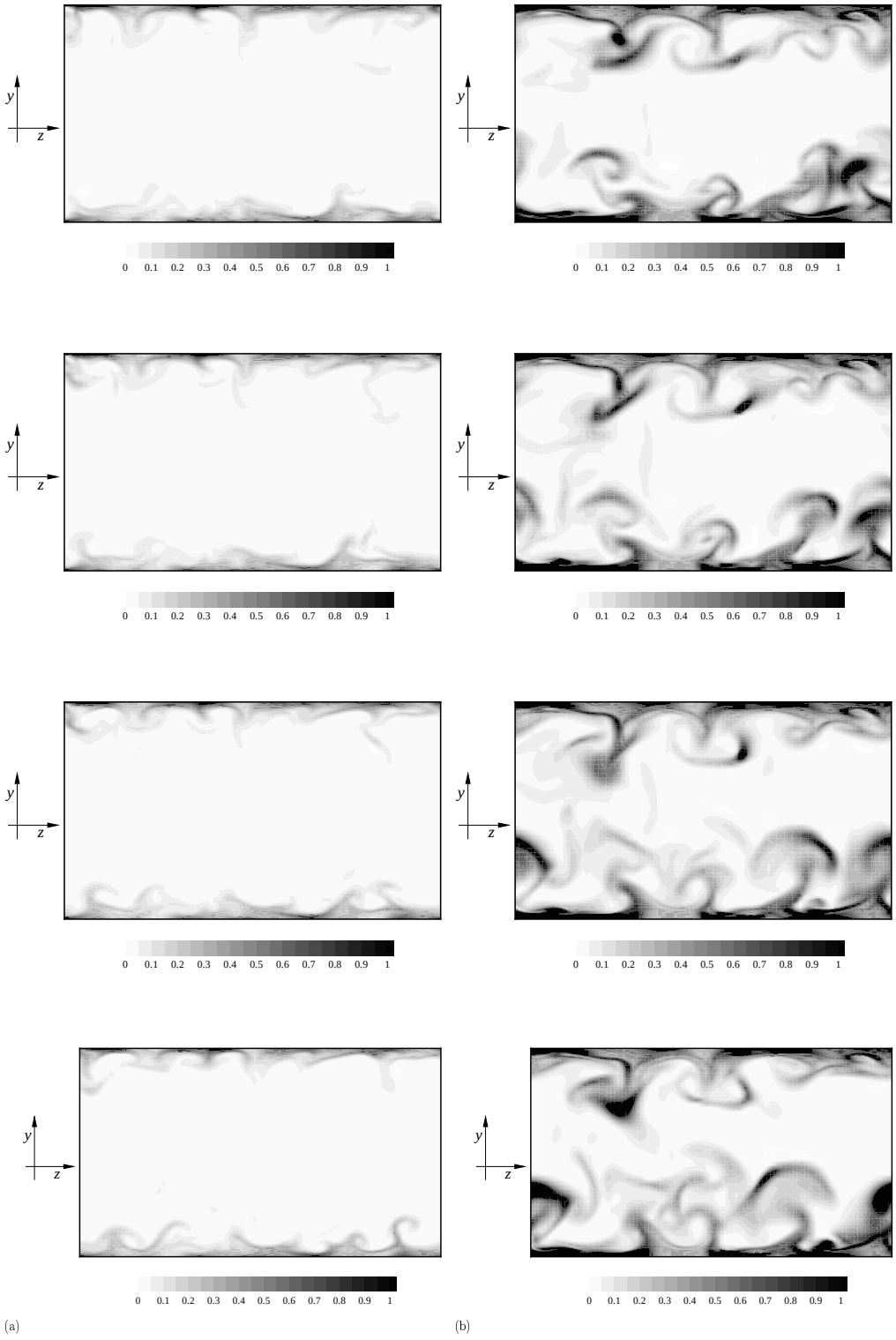

FIGURE 14. Time sequence of the instantaneous elastic energy k_p normalized by $u_{\tau_0}^2$ in a coordinate moving with the structures at $Re = 3000$: (a) $We = 1$; (b) $We = 3$. The time interval between the consecutive instants is 0.2.

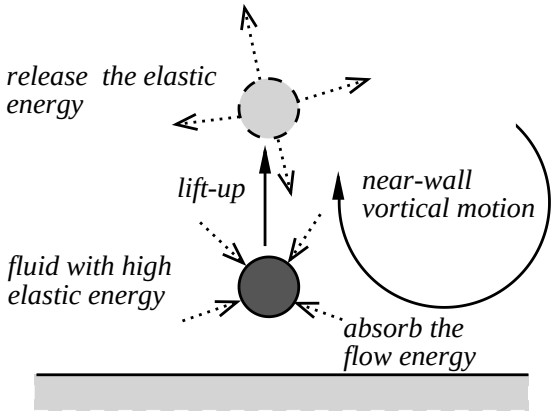

FIGURE 15. Schematic representation of the present drag reduction mechanism.

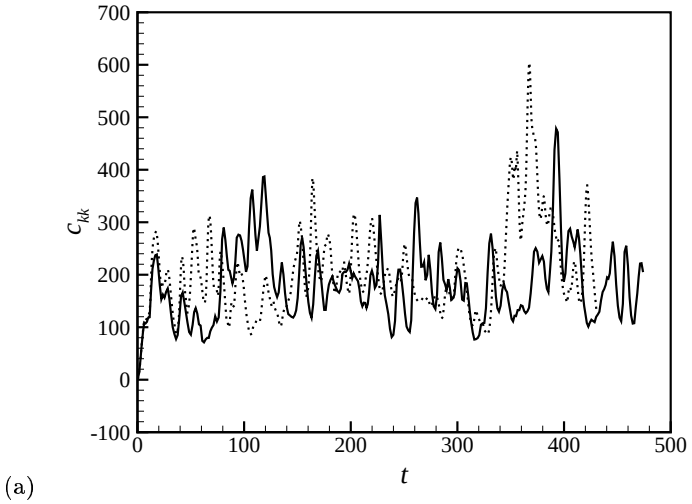

(a)

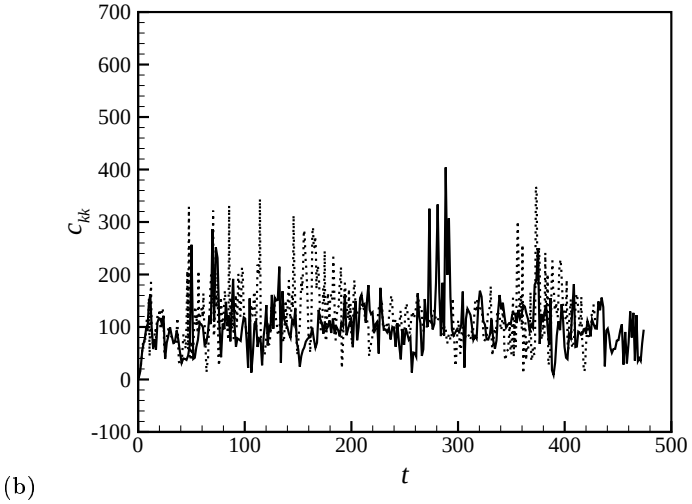

(b)

FIGURE 16. Time histories of the polymer stretch c_{kk} at $Re = 3000$ and $We = 2$: (a) $y_0^+ = 0.2$; (b) $y_0^+ = 10$. ——, FENE-P model with $L^2 = 3600$; ·····, Oldroyd-B model.

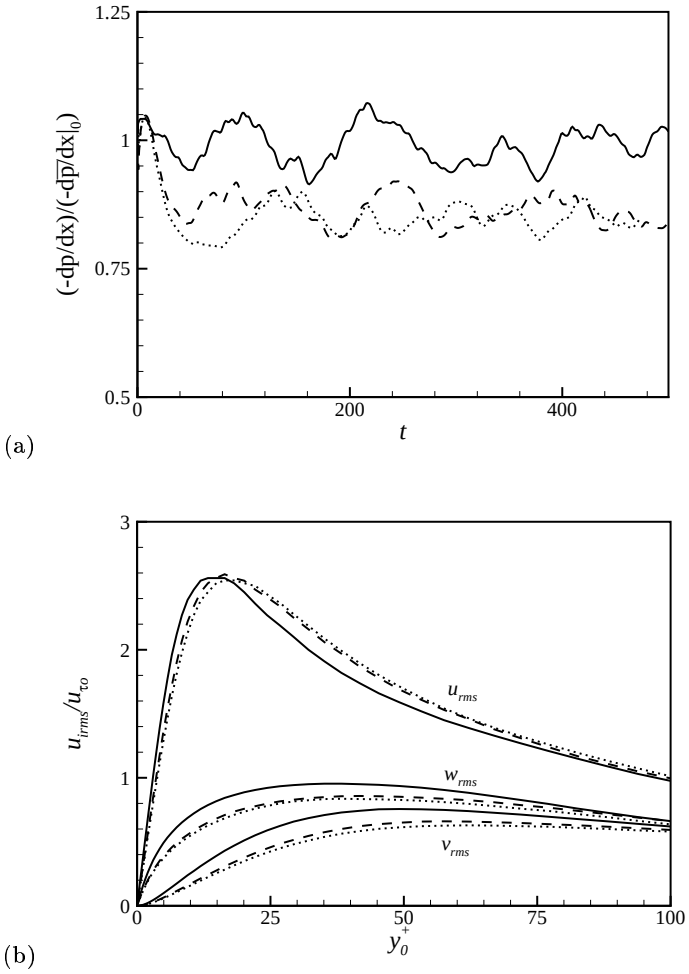

FIGURE 17. Comparison of the results from the Oldroyd-B and FENE-P models at $Re = 3000$ and $We = 2$: (a) time histories of the mean pressure gradient normalized by that of Newtonian fluid flow; (b) root-mean-square velocity fluctuations normalized by the wall-shear velocity u_{τ_0}. ——, Newtonian; – – –, Oldroyd-B model; ·····, FENE-P model with $L^2 = 3600$.